Effect of Equivalence Ratio on Premixed Flame Response to Unsteady Strain-Rate and Curvature

H.N. Najm*, P.S. Wyckoff
Sandia National Laboratories
Livermore, CA 94551

and

O.M. Knio
The Johns Hopkins University
Baltimore, MD 21218-2686

Paper submitted to the 27^{th} International Symposium on Combustion.
University of Colorado, Boulder, CO.
August 2-7, 1998.

Word Length: Text: 4120, Figures: 1200, Tables: 200.

Total: 5520.

Method: unix word count.

Presentation preference: Oral presentation.

Colloquium topic area preference: Laminar flames.

* Corresponding Author, Sandia National Laboratories, P.O.Box 969, MS 9051, Livermore, CA 94551, USA. Tel/Fax: (510) 294-2054/2595, email: hnnajm@ca.sandia.gov

DISCLAIMER

Abstract

The interaction of a premixed stoichiometric methane-air flame with a two-dimensional counter-rotating vortex pair is studied under stoichiometric and rich conditions using a detailed C_1C_2 chemical mechanism. The focus is on the effect of equivalence ratio on flame response to unsteady strain-rate and curvature. Flame structure and transient response are studied, both at curved cusps and on the vortex-pair centerline. The rich flame is found to exhibit faster response to flow disturbances. Results suggest this is due to the increased sensitivity of the flame to H concentration at rich conditions. Significant differences are observed in the unsteady behaviour of some C_2 species, where substantial transient accumulation is observed at stoichiometric conditions, but not at rich conditions. Transient response of flame observables, such as CH, OH, and HCO, is studied and compared to experimental data.

Introduction

The dynamical response of flames in turbulent reacting flow involves complex interactions between unsteady flow structures and flame chemistry. Two essential features of such interactions are the unsteady strain-rate and curvature disturbances to the reaction zone. In this work, we focus on a single flow length/time scale feature in two dimensions (2D), and its effect on a premixed flame for a range of mixture conditions. We study the interaction of a premixed freely propagating methane-air flame with a 2D counter-rotating vortex pair.

There have been both experimental [1,2,3,4,5] and numerical [6,7,8,9,10] studies of these flows. However, much of the existing numerical data is concerned with single-step kinetics, flow dynamics, and thermal effects, rather than flame chemical response. Exceptions include one-dimensional (1D) studies of opposed-jet flames [11,12] with sinusoidal perturbations, as well as 2D turbulence studies [13]. These and other relevant studies will be considered below in the evaluation of the present results.

In earlier work [9,10], we studied the flame/vortex-pair interaction using C_1 kinetics at stoichiometric conditions. As the vortex pair penetrates into the flame, the reaction zone is observed to shift into the products, leading to the depletion of H, O and OH, and the consequent general drop in reaction rates. On the other hand, focusing or defocusing of the diffusive fluxes of H and its precursors in curved flame regions were found to have a significant effect on local flame structure and burning rate. These results were extended to more detailed kinetics, using other C_1 and C_2 mechanisms [14], which investigated the effect of choice of the chemical mechanism on the transient flame response.

The present work investigates the dependence of flame response on equivalence ratio, Φ. Flame interaction with the vortex-pair is computed using C_1-C_2 kinetics for two cases: one stoichiometric at $\Phi = 1.0$, and the other rich at $\Phi = 1.2$. The transient response of selected radicals and species on key hydrocarbon reaction pathways is studied and compared to experimental data. We find that the rich flame has a faster chemical response to flow disturbances. This is in contrast to earlier 1D flame studies [11], where slower response was observed in the thicker rich flame, and was attributed to diffusional transport, rather than chemistry. Present results suggest that the faster chemical response in the rich flame is due to the increased relative influence of H on flame chemistry at rich conditions.

Model Formulation

The governing equations are presented in their non-dimensional form in 2D. The assumptions of zero bulk viscosity [15], negligible body forces, and low Mach number [16] give the conservative continuity and momentum equations:

$$\frac{\partial \rho}{\partial t} + \nabla \cdot (\rho \mathbf{v}) = 0 \tag{1}$$

$$\frac{\partial(\rho u)}{\partial t} + \frac{\partial(\rho u^2)}{\partial x} + \frac{\partial(\rho uv)}{\partial y} = -\frac{\partial p}{\partial x} + \frac{1}{Re}\Phi_x \tag{2}$$

$$\frac{\partial(\rho v)}{\partial t} + \frac{\partial(\rho vu)}{\partial x} + \frac{\partial(\rho v^2)}{\partial y} = -\frac{\partial p}{\partial y} + \frac{1}{Re}\Phi_y \tag{3}$$

where ρ is the density, $\mathbf{v} = (u, v)$ is the velocity vector, p is the pressure, Re is the Reynolds number, and Φ_x,Φ_y are the viscous stress terms.

We assume a detailed chemical reaction mechanism involving N species and M elementary reactions. The energy equation is developed allowing for variable transport properties, and a constant stagnation pressure p_o, *i.e.* an open domain. We neglect Soret and Dufour effects [17] and radiant heat transfer, and assume a perfect gas mixture, with individual species molecular weights, specific heats, and enthalpies of formation, using Fickian binary mass diffusion. The low-Mach-number energy equation is:

$$\frac{\partial T}{\partial t} = -\mathbf{v} \cdot \nabla T + \frac{1}{RePr}\frac{\nabla \cdot (\lambda \nabla T)}{\rho c_p} + \frac{1}{ReSc}\frac{\mathbf{Z} \cdot \nabla T}{c_p} + Da\frac{w_T}{\rho c_p} \tag{4}$$

where T is the temperature, λ is the thermal conductivity, $w_T = -\sum_{i=1}^{N} h_i w_i$ is the chemical heat release source term, h_i is enthalpy, w_i is the production rate of species i, c_p is the mixture specific heat at constant pressure, Pr, Sc, and Da are the Prandtl, Schmidt, and Damköhler numbers respectively, and $\mathbf{Z} = \sum_{i=1}^{N} c_{p,i} D_{iN} \nabla Y_i$. The N-th species, here N_2, is assumed dominant such that the diffusion velocity of any other species i in the mixture is approximated by $\mathbf{V}_i = -D_{iN}\nabla Y_i / Y_i$, where D_{iN} is the binary mass diffusion coefficient of species i into the N-th species, and Y_i is the mass fraction of species i. $\mathbf{V}_N$ is found from the identity $\sum_{i=1}^{N} Y_i \mathbf{V}_i = 0$. For computational efficiency, mixture transport properties (μ,λ) are set to those of the dominant species at the local temperature.

The i-th species conservation equation, for $i = 1, \ldots, N-1$, is written as

$$\frac{\partial(\rho Y_i)}{\partial t} = -\nabla \cdot (\rho \mathbf{v} Y_i) + \frac{1}{ReSc}\nabla \cdot (\rho D_{iN} \nabla Y_i) + Da\ w_i, \tag{5}$$

and the mass fraction Y_N is found from the identity $\sum_{i=1}^{N} Y_i = 1$.

The perfect gas state equation is: $p_o = \rho T/\overline{W}$, where $\overline{W} = 1/\sum_{i=1}^{N}(Y_i/W_i)$, is the local effective molar mass of the mixture. The production rate for each species is given by the sum of contributions of elementary reactions [17], with Arrhenius rates $r_k = A_k T^{b_k} e^{-E_k/RT}$, $k = 1 \ldots M$, including forward and backward rates, and third-body efficiencies [18].

Numerical Scheme

The above equations are solved using a second-order predictor-corrector finite difference projection scheme. The projection method was first introduced by Chorin [19], and is discussed more recently by Kim & Moin [20]. McMurtry *et al.* [21] presented a formulation for reacting flow, using the continuity equation to update the density field. The present method follows more closely that of [7,22], in using the energy equation.

The non-stiff version of this scheme is presented in detail in [9], and has been used to study premixed methane-air flames under stoichiometric conditions [9,10]. The present work uses a stiff scheme which employs an additive (non-split) semi-implicit formulation of the scalar conservation equations in the corrector step. The formulation and convergence of the stiff scheme are discussed in [23]. In the following, the general outline is presented for completeness.

An open 2D rectangular domain is considered, and is overlaid by a uniform mesh. Velocity components are evaluated at cell edges, while other fields are evaluated at cell centers. Spatial derivatives are discretized using second-order central differences, and a second-order Adams-Bashforth (AB2) scheme is used for explicit time integration. Stiff integration of chemical source terms is done using DVODE [24], an ODE integration package. The numerical solution for each time step, from t_n to t_{n+1}, involves the following steps [23]:

1. **Predictor**
   - Evaluate predicted $\tilde{\rho}^{n+1}$, and $\tilde{Y}_i^{n+1}$, using AB2 integration of the scalar conservation equations.
   - Evaluate predicted $\tilde{T}^{n+1}$ from the state equation.
   - Evaluate predicted $\tilde{\mathbf{v}}^{n+1}$ using a variable-density projection scheme[10].
2. **Corrector**
   - Evaluate scalar time gradients, the right-hand-sides of the scalar conservation equations, from the predicted fields at t_{n+1}.
   - Evaluate corrected ρ^{n+1}, and Y_i^{n+1} using the stiff ODE integrator DVODE, operating on a semi-implicit discretization of scalar conservation equations. This uses a second order quasi Crank-Nicolson differencing [25] of the convection and diffusion terms based on their values at t_n and their predicted values at t_{n+1}, added to an implicit

formulation for the chemical source terms. Thus, for the scalar vector $\phi = \{\rho, \rho Y_i\}$, the following ODE system is integrated in each computational cell from t_n to t_{n+1},

$$\frac{\partial \phi}{\partial t} = \frac{1}{2}(C^n + \tilde{C}^{n+1}) + \frac{1}{2}(D^n + \tilde{D}^{n+1}) + R(\phi) \tag{6}$$

where C, D, R, are the convection, diffusion, and reaction right-hand-side terms of the scalar conservation equations. Note that, except for $R(\phi)$ every term on the right-hand-side of (6) is a known constant for the purpose of ODE integration.

- Evaluate corrected T^{n+1} from the state equation.
- Evaluate corrected $\mathbf{v}^{n+1}$ using a variable-density projection scheme[10].

Results

We first examine the effect of equivalence ratio, Φ, on a steady 1D premixed freely propagating methane-air flame. We use a 20% N_2-diluted methane-air mixture at room temperature and atmospheric pressure, in an open domain. Chemkin [18,26] is used to compute the 1D flame solution, with the GRImech1.2 [27] C_1C_2 chemical mechanism. The change in equivalence ratio from stoichiometric ($\Phi = 1.0$) to rich ($\Phi = 1.2$) leads to a drop in peak flame heat release rate w_T by roughly 40% ($\Delta w_T/w_T = -41\%$). The corresponding relative changes in peak mole fractions of a number of selected species are listed in Table I. Note the large drops in O-bearing radicals (O, OH) due to the dearth of O_2 in the rich flame, while a small increase in H and a large increase in H_2 are evident. A significant increase is also observed in CH_3, along with larger increases in C_2 species concentrations. Remarkably, a four-fold increase is observed in C_2H_2. It is reasonable to attribute this large increase in C_2 species to both increased production because of increased CH_3, and decreased consumption because of reduced O and O_2 concentrations. Moreover, note the relative drop of 43% in HCO mole fraction, not far from the 41% drop in heat release. As noted in [10], HCO mole fraction is found to correlate well with changes in heat release rate. On the other hand, note the *increase* in CH mole fraction, as would be expected from the increased equivalence ratio. This indicates that peak CH mole fraction may not be a good measure of heat release rate, even in this steady 1D flame.

Consider next the interaction of the above premixed methane-air flame with a counter-rotating vortex pair. An open rectangular domain is considered, with dimensions 0.4×1.6 cm, and is overlaid by a 256×1024 uniform mesh. We apply symmetry boundary conditions in the horizontal x-direction, and outflow boundary conditions in the y-direction. The evolution of the flow over a 1 ms time span is illustrated in Figures 1 and 2 for the stoichiometric and rich flames respectively. The vertical right edge of the domain is the centerline of the vortex pair under consideration, which is one member of an infinite periodic row of vortex pairs along the horizontal x-direction. The initial condition is a superposition of the velocity (u,v) field induced by the periodic row of vortex pairs, and the temperature, density and mass fraction (T,ρ,Y_i) distributions corresponding to a horizontal premixed flame, with the initial structure in the y-direction from the above 1D flame solution.

The flame propagates downward by burning into the reactants, as shown in Figs. 1 and 2. The vorticity field causes significant contortion of the flame as the vortex pair propagates upwards into it. A baroclinic vorticity dipole is generated in the neighborhood of the original vortex, in agreement with the numerical results of [6,7,9] and the measurements of Mueller *et al.* [5]. This vortical fluid is entrained into the vortex pair in a continuing process that leads to the generation of multiple folds of counter-rotating vorticity inside the original vortex. The flow dynamics reflect the relative disparity between flame and vortex-pair time scales, the ratio of which yields a Damköhler number $Da = 0.04 \ll 1$.

The heat release rate decays significantly along the flame length due to the strain-rate and curvature disturbances. Strongest decay is observed on the centerline and around the vortex pair, consistent with the higher strain-rate in these regions. The rich flame exhibits more significant decay of heat release than the stoichiometric flame, both on centerline and along the whole flame length. This increased susceptibility to the flow is consistent with the lower burning rate in the rich flame. It is also evident that the flame contortion in the wake of vortex-pair is more severe in the rich case. This may be attributed to: (1) lower heat release and expansion rates in the rich flame and the consequent reduction in attenuation of vortex structures; and (2) the higher burning speed of the stoichiometric flame, which allows it to burn faster through negatively curved regions (concave towards the reactants) to achieve a less contorted shape. On the other hand, both flames exhibit qualitatively similar behaviour in the curved regions, with a minimum burning rate at the positively curved cusp and a maximum at the negatively curved cusp. These variations are evident in the heat release rate data in Figs. 1 and 2. Consistent with our earlier observation in [9], we find a maximum/minimum in H production/consumption rate, on the products/reactants side of the flame at the positive cusp. Conversely, a maximum in H consumption rate is observed on the reactants side of the flame at the negatively-curved cusp. This, along with the associated local increase in burning rate, evidently leads to a peak in H production on the products side of the flame at the negative cusp. Thus both production and consumption of H peak at the negatively curved flame location, consistent with [13]. This holds both for the stoichiometric and rich flames, although the effect is more accentuated in the rich case because of the increased curvature and enhanced flame susceptibility to flow disturbances.

Consider next the flame response on the vortex-pair centerline. The process by which

flame burning rate decays at this location is associated, both for the stoichiometric and rich case, with a shift of the reaction zone into the products as observed in [9], resulting in increased CO_2 concentration and temperature (and reduced O_2 concentraion) in the reaction zone, as the burning and heat release rates plummet. This shift into the hot products leads to a drop in H production rates, as well as lower O and OH production (through chain-branching reactions), resulting in an overall drop in burning rate.

The evolution of peak heat release rate on the centerline is illustrated in Figure 3, where faster decay rate is observed for the rich flame. Given that the flame topology and strain-rate at this location are similar in the two cases, the observed trend suggests that the rich flame has a faster response time. In contrast, previous sinusoidally-perturbed 1D opposed-jet premixed flame data [11] suggests faster response time from the stoichiometric flame. This observation was attributed to the enhanced burning rate at $\Phi = 1.0$ and the resulting thinner flame profiles, and smaller diffusive transport times. The present flow involves non-linear transient flame response to a large-amplitude strain-rate ($\approx 5000\,\mathrm{s}^{-1}$) imposed in the reaction zone at $t = 0$. Thus, the results pertain more to the chemical time response of the flame, rather than diffusional transport time in the preheat zone. This, and the fact that the present flame is not constrained between opposed jets, and that different chemical mechanisms were used, makes direct comparison to the 1D results difficult. On the other hand, the observed faster response of the rich flame suggests an important role for chemistry, rather than diffusion, in the present flame time response.

To investigate the transient roles played by individual reactions and species, a fractional influence analysis [9] is used, incorporating sensitivity data, at time 0.5 ms. The fractional influence due to each species/temperature on a given reaction is defined as the change in reaction rate resulting from the change in the particular species concentration or temperature. The total change in the rate of progress $\mathcal{R}_k$ of the k-th reaction (Rn.(k)) between two time instances is given by : $\Delta\mathcal{R}_k = \sum_j (\partial\mathcal{R}_k/\partial\zeta_j)\Delta\zeta_j$ where $\zeta = \{c_1, \cdots, c_N, T\}$, and c_j is the concentration of species j. The corresponding total change in production rate of species i is given by : $\Delta w_i = \sum_k \nu_{ik}\Delta\mathcal{R}_k = \sum_j \Delta\zeta_j(\sum_k \nu_{ik}\partial\mathcal{R}_k/\partial\zeta_j)$, where ν_{ik} is the stoichiometric coefficient of species i in reaction k.

Consider then the transient response of OH, O, and H, in the stoichiometric and rich flames, shown in Figure 4. Clearly, OH and O mole fractions decay faster in the rich case,

while the decay rate of H is roughly unchanged. To explain this faster response of OH and O, we use fractional influence analysis to examine the contributions of relevant species to Δw_i. The results indicate that the fractional influence of H on changes in OH-production rate is more dominant at $\Phi = 1.2$, relative to the influences of OH and O. At $\Phi = 1.0$ peak OH mole fraction decays relatively slowly compared with that of H, as seen in Fig. 4, because of the dominance of its own influence on Δw_{OH}, and the significance of others such as O, H_2, and T, relative to H. On the other hand, OH decays faster in the rich case, at a rate comparable to the fast H decay rate, because of the increased fractional influence of H on Δw_{OH}, relative to that of OH itself, O and others. This increased role of H is consistent with the above discussed change in the steady state 1D flame structure in going from stoichiometric to rich conditions. Given the scarcity of OH and O in the rich flame, it would be expected that this flame has increased reliance on H to move carbon down the reaction pathways, many of which can proceed with either OH or H. These observations are also true in the case of O, which exhibits faster response at rich conditions. Moreover, this increased role of H is also observed for hydrocarbon species such as CH_3, C_2H_6-C_2H_3, CH, and HCO. This increased influence of H on changes in production rates of hydrocarbons in the rich flame, as well as the faster response of OH and O, leads to a faster response in the overall burning and heat release rates.

The response of particular hydrocarbon species can vary widely for the two flames. As shown in Figure 5, CH_3 mole fraction exhibits a transient rise before proceeding to decay, for $\Phi = 1.0$, whereas its response in the rich flame shows monotonic decay. CH and HCO mole fractions exhibit monotonic decay in both cases, with faster decay rate for the rich flame.

Recent Planar Laser Induced Fluorescence (PLIF) experimental evidence from a V-flame interaction with a vortex-pair at similar N_2-diluted stoichiometric mixture conditions [4,10] suggests that peak CH decays significantly faster than HCO on the vortex-pair centerline. The present results in Fig. 5 clearly exhibit the opposite trend. Moreover, the same experiment indicates that at $\Phi = 1.2$, peak OH exhibits a large rise by nearly a factor of 3, simultaneous with the drop in CH, before proceeding to decay. This OH "burst" has not been observed in the present results, as can be seen in Fig. 4. Further, Ngyuen and Paul [4] find that, while the transient burst in OH observed at rich conditions is on the same time scale as CH, the OH decay rate at stoichiometric conditions (or subsequent to this burst at

rich conditions) occurs at a much longer time scale. On the other hand, Figs. 4 and 5 show that CH and OH have similar response times.

Fractional influence analysis can identify reactions whose rate constants may have a significant role in these discrepancies. Results indicate that, for both $\Phi = 1.0$ and 1.2, the largest three $\Delta\mathcal{R}_k$ contributors to Δw_{CH} are (in order of decreasing peak $|\Delta\mathcal{R}_k|$): Rn.(-126): $\mathrm{H} + \mathrm{CH_2} \Longleftrightarrow \mathrm{CH} + \mathrm{H_2}$, Rn.(127): $\mathrm{CH} + \mathrm{H_2O} \Longleftrightarrow \mathrm{H} + \mathrm{CH_2O}$, and Rn.(125): $\mathrm{CH} + \mathrm{O_2} \Longleftrightarrow \mathrm{O} + \mathrm{HCO}$. The labels indicate reaction numbers in GRImech1.2 [27], and a negative reaction number indicates that the reaction is written inverted from its original listing in the mechanism. Similarly, for OH, the top three $\Delta\mathcal{R}_k$ reactions at $\Phi = 1.0$ are: Rn.(38): $\mathrm{H} + \mathrm{O_2} \Longleftrightarrow \mathrm{O} + \mathrm{OH}$, Rn.(98): $\mathrm{OH} + \mathrm{CH_4} \Longleftrightarrow \mathrm{CH_3} + \mathrm{H_2O}$, and Rn.(84): $\mathrm{OH} + \mathrm{H_2} \Longleftrightarrow \mathrm{H} + \mathrm{H_2O}$, with Rns.(84) and (98) switching ranks at $\Phi = 1.2$, consistent with the above enhanced role of H in the rich flame. As for HCO, the top three Rns. at $\Phi = 1.0$ are: Rn.(166): $\mathrm{H} + \mathrm{CO} + \mathrm{H_2O} \Longleftrightarrow \mathrm{HCO} + \mathrm{H_2O}$, Rn.(101): $\mathrm{OH} + \mathrm{CH_2O} \Longleftrightarrow \mathrm{HCO} + \mathrm{H_2O}$, and Rn.(58): $\mathrm{H} + \mathrm{CH_2O} \Longleftrightarrow \mathrm{HCO} + \mathrm{H_2}$. At $\Phi = 1.2$, Rn.(101) has a relatively minor role, with Rn.(58) in rank 2, and Rn.(167): $\mathrm{HCO} + \mathrm{M} \Longleftrightarrow \mathrm{H} + \mathrm{CO} + \mathrm{M}$ in rank 3, again consistent with enhanced influence of H.

The evolution of peak mole fractions of selected C_2 species are shown in Figure 6. Note the large change in the dynamic response of $\mathrm{C_2H_2}$ for the two cases. For $\Phi = 1.0$, $\mathrm{C_2H_2}$ mole fraction rises by a factor of 2.5 after 1 ms, whereas a gradual decay from the initial value is observed for $\Phi = 1.2$. $\mathrm{C_2H_3}$ decays in time for both stoichiometric and rich cases, with a faster decay rate in the rich case. $\mathrm{C_2H_6}$ mole fraction decays monotonically for both cases, again with faster rate of decay in the rich flame.

This significant transient rise in $\mathrm{C_2H_2}$ mole fraction in the stoichiometric case, and its absence from the rich case, is of interest, given the relevance of $\mathrm{C_2H_2}$ to soot production. We find that the causes for both observations relate to the differences in the rates of decay of $\mathrm{C_2H_3}$ and H concentrations. The largest $\Delta\mathcal{R}_k$ contributor to $w_{\mathrm{C_2H_2}}$ is Rn.(-71): $\mathrm{C_2H_3(+M)} \Longleftrightarrow \mathrm{H} + \mathrm{C_2H_2(+M)}$. At $\Phi = 1.0$, the rate of decay of peak $\mathrm{C_2H_3}$ is actually slower than the rate of decay of H. Thus, even though the forward rate of Rn.(-71) is falling, its reverse rate is falling faster, resulting in a net speedup in the foward direction, towards increased $w_{\mathrm{C_2H_2}}$. The opposite happens at rich conditions, resulting in a net drop in $w_{\mathrm{C_2H_2}}$.

Conclusions

We studied the effect of equivalence ratio on the transient response of a 2D premixed methane-air flame under large flow perturbations. Generally, the rich flame is found to be more susceptible to flow disturbances. Results indicate significant qualitative and quantitative changes in detailed flame response depending on equivalence ratio.

We observe a faster response time in the rich flame, with faster decay of species mole fractions and overall heat release rate. Comparison to existing 1D flame data suggests a chemical rather than diffusional cause for this behaviour. Results suggest that the faster chemical response of the rich flame is due to the increased relative influence of H under rich conditions, and therefore the dominance of the faster H time scale.

Evolution of flame radicals and burning rate reaches a plateau earlier in the stoichiometric case. Both cases seem to reach a non-zero burning rate plateau, suggesting that this flame may not fully extinguish in either case without a radiation heat loss term in the model.

Some C_2 species were observed to exhibit significant transient accumulation at stoichiometric, but not at rich, conditions. A large transient increase in C_2H_2 concentration was observed, driven by subtle differences in the decay rate of concentrations of C_2H_3 and H.

Discrepancies between computed relative response times of CH, OH, and HCO, and experimental data were observed. Additional work is necessary to suggest required modifications to the model to provide a more accurate dynamical flame response. These may include improvements in reaction rate constants, the set of species and reactions, transport or thermodynamic property models, or all of the above Generally, these observations highlight the need for characterization of the time response of chemical mechanisms.

Acknowledgments

This work was supported by the US Department of Energy (DOE), the DOE Office of Basic Energy Sciences, Chemical Sciences Division, and the DOE Defense Programs Accelerated Strategic Computing Initiative (ASCI).

References

[1] Roberts, W.L., Driscoll, J.F., Drake, M.C., and Goss, L.P., *Combustion and Flame*, 94:58–69 (1993).

[2] Samaniego, J.-M., Annual research briefs, Center for Turbulence Research, Stanford University/NASA Ames Research Center, (1993).

[3] Mueller, C.J., Driscoll, J.F., Sutkus, D.J., Roberts, W.L., Drake, M.C., and Smooke, M.D., *Combustion and Flame*, 100:323–331 (1995).

[4] Nguyen, Q.-V., and Paul, P.H., *Twenty-Sixth Symposium (International) on Combustion*, The Combustion Institute, 1996, , pp. 357–364.

[5] Mueller, C.J., Driscoll, J.F., Reuss, D.L., Drake, M.C., and Rosalik, M.E., *Combustion and Flame* (1996) in press.

[6] Ashurst, W.T., and McMurtry, P.A., *Combustion Science and Technology*, 66:17–37 (1989).

[7] Rutland, C.J., and Ferziger, J.H., *Combustion and Flame*, 84:343–360 (1991).

[8] Poinsot, T., Veynante, D., and Candel, S., *J. Fluid Mechanics*, 228:561–606 (1991).

[9] Najm, H.N., and Wyckoff, P.S., *Combustion and Flame*, 110(1-2):92–112 (1997).

[10] Najm, H.N., Paul, P.H., Mueller, C.J., and Wyckoff, P.S., *Combustion and Flame* (1997) in press.

[11] Egolfopoulos, F.N., *Twenty-Fifth Symposium (International) on Combustion*, The Combustion Institute, 1994, , pp. 1365–1373.

[12] Petrov, C.A., and Ghoniem, A.F., *Combustion and Flame*, 102:401–417 (1995).

[13] Echekki, T., and Chen, J.H., *Combustion and Flame*, 106:184–202 (1996).

[14] Wyckoff, P.S., and Najm, H.N., *Chemical and Physical Processes in Combustion*, 1996 Fall Technical Meeting, The Eastern States Section of the Combustion Institute, December 9-11, Hilton Head, SC, 1996, , pp. 67–70.

[15] Schlichting, H., *Boundary-Layer Theory,* McGraw-Hill, New York, 7^{th} edition, 1979.

[16] Majda, A., and Sethian, J., *Combustion Science and Technology*, 42:185–205 (1985).

[17] Williams, F.A., *Combustion Theory,* Addison-Wesley, New York, 2nd edition, 1985.

[18] Kee, R.J., Rupley, F.M., and Miller, J.A., Sandia Report SAND89-8009B, Sandia National Labs., Livermore, CA., (1993).

[19] Chorin, A.J., *J. Comput. Phys.*, 2:12–26 (1967).

[20] Kim, J., and Moin, P., *J. Comput. Phys.*, 59:308–323 (1985).

[21] McMurtry, P.A., Jou, W.-H., Riley, J.J., and Metcalfe, R.W., *AIAA J.*, 24(6):962–970 (1986).

[22] Mahalingam, S., Cantwell, B.J., and Ferziger, J.H., *Physics of Fluids A*, 2:720–728 (1990).

[23] Najm, H.N., Wyckoff, P.S., and Knio, O.M., *Journal of Computational Physics* (1997) in press.

[24] Brown, P.N., Byrne, G.D., and Hindmarsh, A.C., *SIAM J. Sci. Stat. Comput.*, 10:1038–1051 (1989).

[25] Anderson, D.A., Tannehill, J.C., and Pletcher, R.H., *Computational Fluid Mechanics and Heat Transfer,* Hemisphere Pub. Co., New York, 1984.

[26] Kee, R.J., Grcar, J.F., Smooke, M.D., and Miller, J.A., Sandia Report SAND85-8240, Sandia National Labs., Livermore, CA., (1993).

[27] Frenklach, M., Wang, H., Goldenberg, M., Smith, G.P., Golden, D.M., Bowman, C.T., Hanson, R.K., Gardiner, W.C., and Lissianski, V., Topical Report GRI-95/0058, Gas Research Institute, (1995).

Table Captions

Table I. Relative changes in peak mole fractions of relevant species corresponding to the change in equivalence ratio from 1.0 to 1.2, for a one-dimensional premixed 20% diluted methane-air flame.

Figure Captions

Figure 1. Evolution of the heat release rate (color) and vorticity fields (contours) for the stoichiometric flame, for a time span of 1 ms. Frames are at 0.2, 0.6, and 1.0 ms. Solid/dashed contours denote positive/negative vorticity.

Figure 2. Evolution of the heat release rate (color) and vorticity fields (contours) for the rich flame with $\Phi = 1.2$, for a time span of 1 ms. Frames are at 0.2, 0.6, and 1.0 ms. Solid/dashed contours denote positive/negative vorticity.

Figure 3. Decay of the peak heat release rate on the vortex-pair centerline for the stoichiometric and rich cases.

Figure 4. Decay of peak mole fractions on the vortex-pair centerline for the stoichiometric and rich cases.

Figure 5. Evolution of peak mole fractions on the vortex-pair centerline for the stoichiometric and rich cases.

Figure 6. Evolution of peak mole fractions on the vortex-pair centerline for the stoichiometric and rich cases.

Species	CH_4	O_2	H	O	OH	CO_2	H_2O
$(\Delta X/X)$ %	+17.7	-1.80	+9.5	-82.0	-58.0	-24.5	+0.80

Species	CH_3	C_2H_6	C_2H_5	C_2H_4	C_2H_3	C_2H_2	C_2H
$(\Delta X/X)$ %	+26.6	+27.6	-5.1	+101	+93.	+444	+278

Species	CH_2O	HCO	CO	H_2	CH_2	CH	C
$(\Delta X/X)$ %	-2.9	-42.6	+42.7	+125	+17.6	+35.1	+347

Table I. Relative changes in peak mole fractions of relevant species corresponding to the change in equivalence ratio from 1.0 to 1.2, for a one-dimensional premixed 20% diluted methane-air flame.

Figure 1. Evolution of the heat release rate (color) and vorticity fields (contours) for the stoichiometric flame, for a time span of 1 ms. Frames are at 0.2, 0.6, and 1.0 ms. Solid/dashed contours denote positive/negative vorticity.

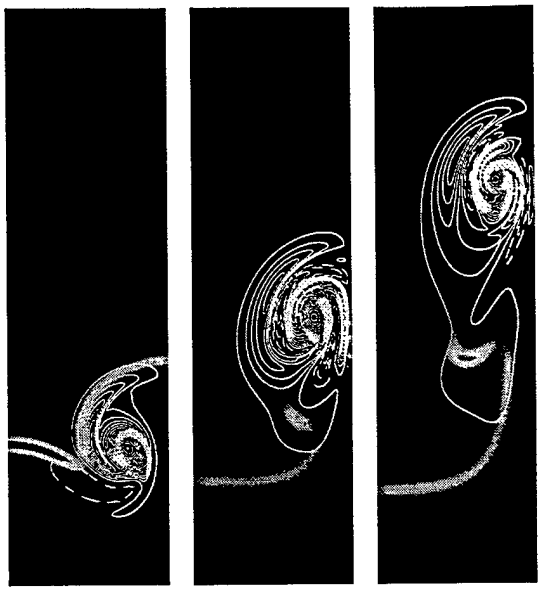

Figure 2. Evolution of the heat release rate (color) and vorticity fields (contours) for the rich flame with $\Phi = 1.2$, for a time span of 1 ms. Frames are at 0.2, 0.6, and 1.0 ms. Solid/dashed contours denote positive/negative vorticity.

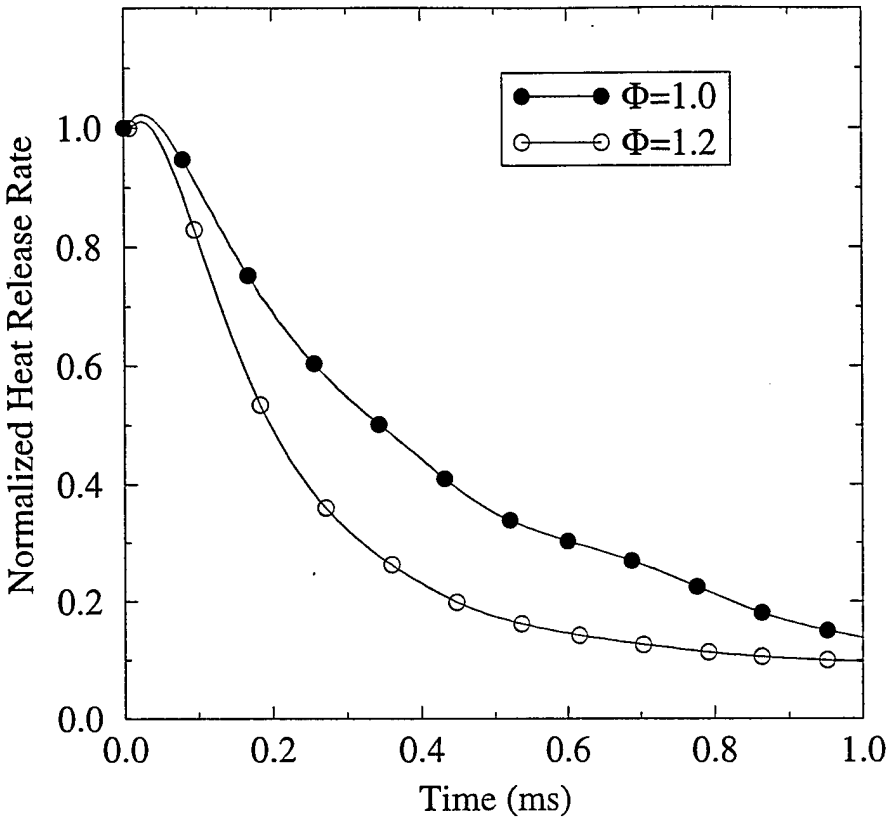

Figure 3. Decay of the peak heat release rate on the vortex-pair centerline for the stoichiometric and rich cases.

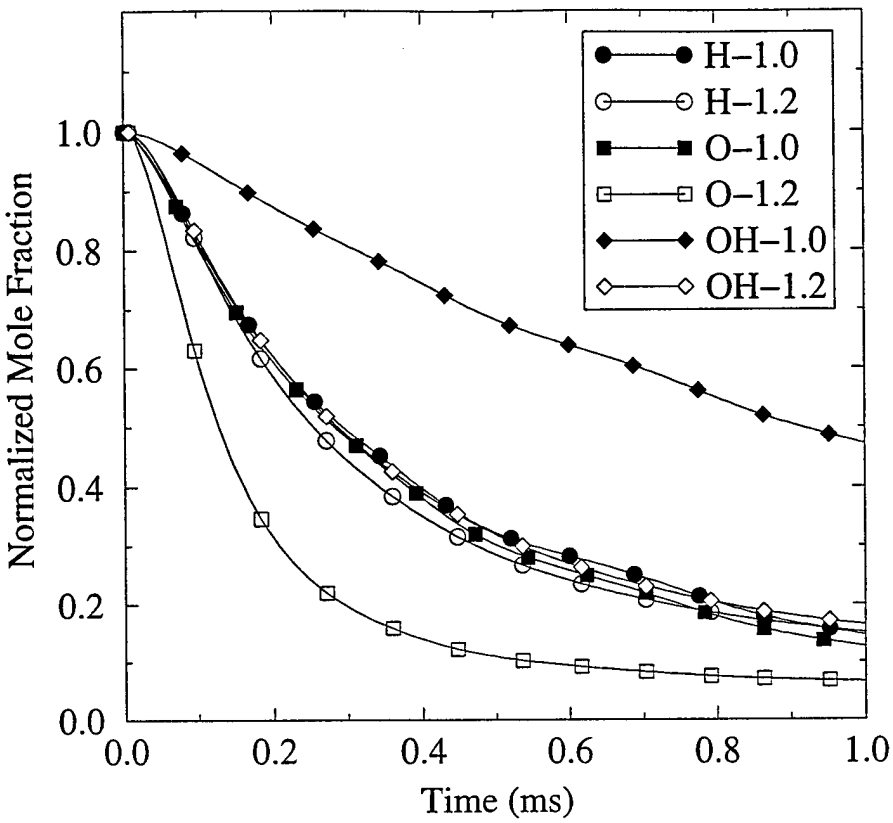

Figure 4. Decay of peak mole fractions on the vortex-pair centerline for the stoichiometric and rich cases.

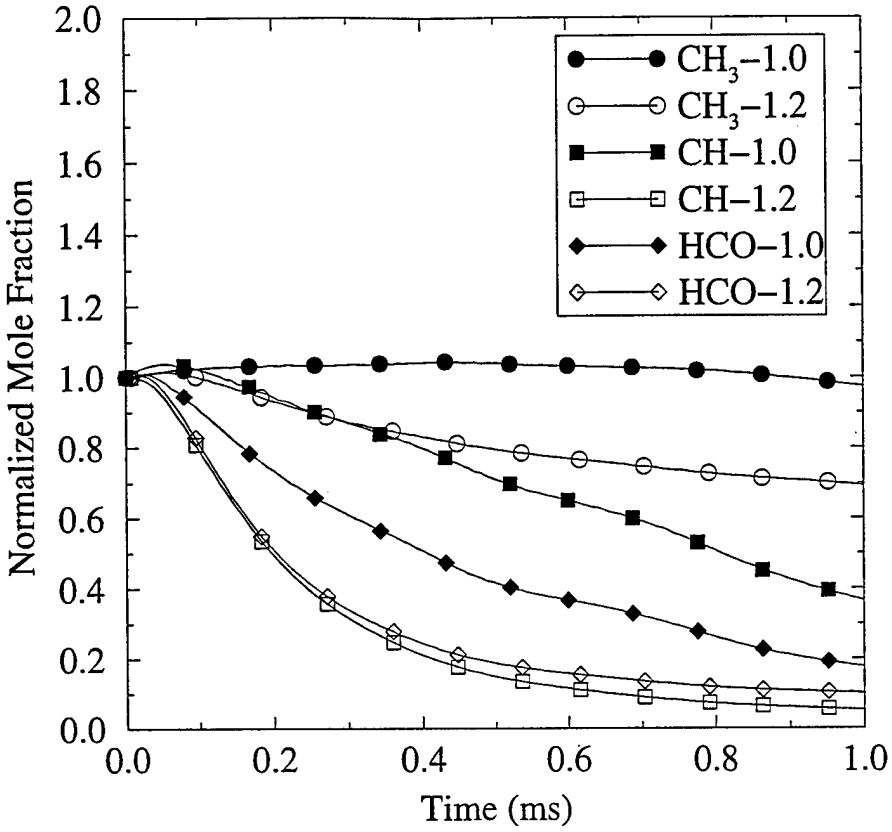

Figure 5. Evolution of peak mole fractions on the vortex-pair centerline for the stoichiometric and rich cases.

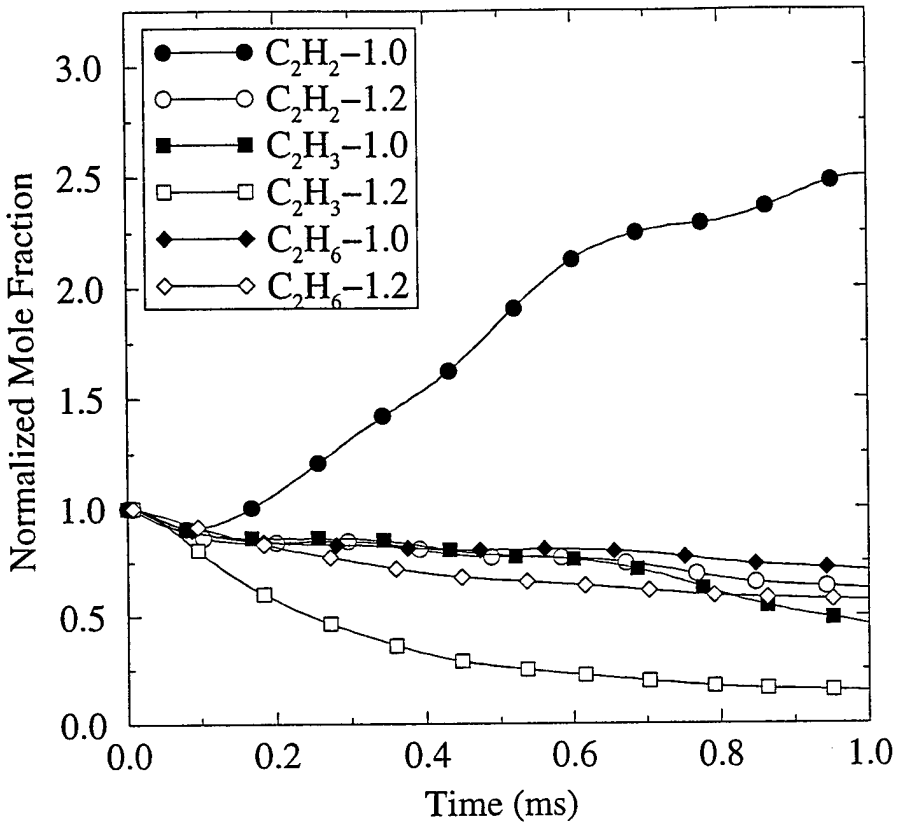

Figure 6. Evolution of peak mole fractions on the vortex-pair centerline for the stoichiometric and rich cases.

Report Number (14) SAND--98-8461C
CONF-980804--

Publ. Date (11) 199808
Sponsor Code (18) DOE/EE, XF
UC Category (19) UC-1409, DOE/ER